ARTICLES

Spatial Bistability in a pH Autocatalytic System: From Long to Short Range Activation

István Szalai,* F. Gauffre, V. Labrot, J. Boissonade, and P. De Kepper

Centre de Recherche Paul Pascal, CNRS Bordeaux, Avennue Schweitzer, F-33600 Pessac, France

Received: May 3, 2005; In Final Form: July 6, 2005

The acid-auto-activated chlorite−tetrathionate reaction is studied in a one-side-fed spatial reactor. It was previously shown that in these conditions the unstirred reaction−diffusion system can generate oscillatory and excitable states even though under well-stirred nonequilibrium conditions only steady-state bistability is observed. Numerical simulations suggest that these temporal reaction−diffusion instabilities result from long-range activation by rapidly diffusing protons. We study here experimentally and numerically the effect of introducing into this reaction−diffusion system macromolecular carboxylate species that reduce the effective diffusivity of protons. Consistent with the original assumption, the introduction of such slow mobility proton-binding species quenches both oscillatory and excitability dynamics. Within the bistability domain the direction of the propagation of an interface between the two steady states depends on control parameter value. We elaborate on the fact that beyond a low critical concentration of macromolecular carboxylate species, the stability limit of the "thermodynamic" branch of spatial steady state does not depend on this concentration. Despite the relative simplicity of the kinetic model used in the numerical simulations, the results are in quasi-quantitative agreement with the experimental observations.

Introduction

Great interest is paid to pattern formation in chemical reacting and diffusing systems. Both their theoretical and experimental studies are a major field of research in nonlinear science.[1−5] Self-organization phenomena in reaction−diffusion systems encompass different types of oscillatory, traveling, and stationary patterns. Reactions leading to such patterns include competing chemical activation and inhibition kinetic pathways. Many families of such reactions are now known.[1,3,6] The temporal and spatial instabilities that lead to the development of patterns crucially depend on the time and space scales over which activation and inhibition processes evolve. Oscillations and travelling wave patterns are associated with time scale separation and are typical of fast activation and slow inhibition systems, while stationary patterns are usually associated with long-range inhibition and short-range activation.[4,5,7] In the simple standard cases, the observation of stationary concentration patterns requires that the activation species, or at least a species controlling the activation kinetic pathway, should have a slower effective diffusivity than the antagonist inhibitory species. Hence, it is of fundamental interest to be able to control the relative space and time scales over which these competing chemical processes operate.

Two different approaches have been developed to selectively control the effective diffusivity of species: (i) First is the addition of uniformly distributed immobile (or reduced mobility) functional sites able to reversibly bind a targeted species. If the targeted species is the activator of the reaction, the effective diffusion of this species decreases, while the others are left unchanged, in particular the inhibitors, which then may have a higher diffusivity than the activator. In addition, if the complex is nonreactive, the apparent reactivity of the activator is reduced and oscillatory states can be quenched.[8,9] (ii) Second is the use of dispersed multiphase systems where some species stay trapped in droplets of the minority phase, while others diffuse in the continuum phase. Presently, the only example of this type is the so-called BZ-AOT system.[10]

At this time, most documented stationary symmetry breaking chemical patterns rely on the presence of binding sites of reduced mobility. It is also the case of interest to us in this work. In this category, only two families of reactions have led to stationary reaction−diffusion patterns in open spatial reactors. One consists of chlorite-iodide driven systems[11] where the activator path is controlled by iodide ions. Using starch or poly(vinyl alcohol) to immobilize these ions in the form of polyiodide complexes, these systems exhibit Turing patterns[12−14] and standing pulses or transient domain patterns[15] when the system displays multiple steady states. The other is the ferrocyanide−iodate−sulfite (FIS) reaction which produces labyrinthine patterns and self-replicating and oscillating spots.[16] The reaction is primarily auto-activated by protons, but iodide ions could also have a secondary auto-activation role.[17] Beside the above-mentioned reactions, only two other reactions have been operated in open spatial gel-reactors: the popular Belousov−Zhabotinsky (BZ)[1,2] reaction under both constant constraints (traveling waves, spiral core dynamics, spiral turbulence)[18−20] or periodic forcing (stationary and traveling resonant patterns)[21] and the chlorite−tetrathionate (CT) reaction.[22,23]

Among the different open spatial reactors developed in recent years, the one-side-fed reactor (OSFR) is the most commonly

* Corresponding author. Permanent address: Department of Inorganic and Analytical Chemistry, L. Eötvös University, P.O. Box 32, H-1518 Budapest 112, Hungary.

10.1021/jp0522922 CCC: $30.25
Published on Web 08/17/2005

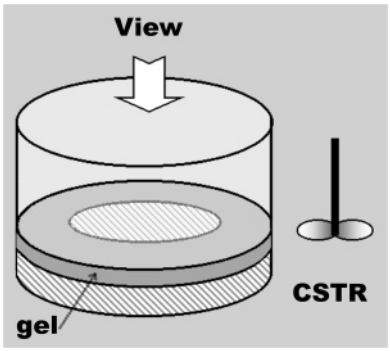

Figure 1. Sketch of the gel core of an annular one-side-fed reactor.

used.[14,16,18] It typically consists of a thin disk of gel fed with fresh reactants by diffusion from one face kept in contact with the contents of a continuous stirred tank reactor (CSTR). The other face of the gel is pressed against an impermeable wall. The gel medium cuts down the hydrodynamic turbulence of the CSTR and preserves diffusive molecular transport. The CSTR ensures constant and uniform feed conditions along the contact boundary with the piece of gel. Beside disk-shaped OSFRs, other geometries have been developed for specific purposes, like the flat annular shape that makes it possible to visualize the chemical concentrations profiles across the depth of the gel. In the present work, we mainly use this geometry of reactor, schematically represented in Figure 1.

It has been shown that reaction systems exhibiting bistability in a CSTR can lead to a phenomenon called "spatial bistability"[24] when they are operated in an OSFR. This phenomenon corresponds to the coexistence of two different concentration profiles across the depth of the gel reactor, for the same fixed composition of the CSTR contents. The phenomenon has been clearly analyzed both from the theoretical and experimental viewpoint for the chlorine dioxide−iodide[24,25] and for the chlorite−tetrathionate[22,23] systems, and is implicit in the FIS reaction experiments.[16]

The present work focuses on the chlorite−tetrathionate (CT) reaction. Though the detailed kinetic mechanism of this reaction is complex, the overall balance equation of the reaction is appropriately represented by

$$7ClO_2^- + 2S_4O_6^{2-} + 6H_2O \rightarrow 7Cl^- + 8SO_4^{2-} + 12H^+ \quad (1)$$

and in a narrow range of stoichiometric conditions, fulfilled in this work, the driving kinetics can be conveniently described by the following empirical rate law:[26]

$$v_k = -\frac{1}{7}\frac{d}{dt}[ClO_2^-] = k[ClO_2^-][S_4O_6^{2-}][H^+]^2 \quad (2)$$

Since in our experiments, the pH of the solution can change from basic to acid, it was shown that to express correctly the overall kinetic process it is also necessary to take into account the fast dissociation equilibria:[22,23]

$$H^+ + OH^- \rightleftharpoons H_2O \quad (3)$$

$$H^+ + SO_4^{2-} \rightleftharpoons HSO_4^- \quad (4)$$

Their rate laws are respectively given by

$$v_e = k_e^+ - k_e^- [H^+][OH^-] \quad (5)$$

$$v_a = k_a^+ [HSO_4^-] - k_a^- [H^+][SO_4^{2-}] \quad (6)$$

This model is profitably used in the theoretical section of this work. When operated in a CSTR, the system exhibits an extended domain of bistability between two steady states separated by large pH differences. In a OSFR, the reaction exhibits a domain of spatial bistability, supplemented by domains of sustained spatiotemporal oscillations and of excitability. Interestingly, these dynamical phenomena do not seem to originate from the sole kinetic mechanism, as observed in other reactions, but are thought to be linked to the fact that the proton, the driving activatory species, diffuses faster than the reagents.[22,23]

Here, we focus on the effect of introducing long polymer chains bearing carboxylate functions on the dynamics of the CT reaction operated in an OSFR. The reversible protonation of carboxylic groups with very reduced mobility can lead to a decrease in the effective diffusivity of protons. Under batch conditions, it is shown experimentally and by simulations that even a small amount of binding agent significantly decreases the diffusitivity of the protons.[27,28] The CT reaction offers a privileged experimental situation where it should be possible to tune the relative activatory/inhibitory space scales from long-range activation and short-range inhibition to short-range activation and long-range inhibition. The addition of a macromolecular carboxylate enables a test of the previously suggested[23] mechanism for the observed oscillations. The experimental results reported in the second section are supported by numerical calculations in the third section. The implications of our observations on colliding fronts are discussed in the last section.

Experimental Conditions

The core of our spatial reactor consists of a flat annular piece of gel tightly inserted into a groove in a polished transparent Plexiglas cylinder immersed in the CSTR contents. The gel annulus, made of a 2% agarose (Fluka 05070) network, has an outer radius $r = 2.5$ cm, a width (the difference between the external and internal radius) $w = 1.0$ mm, and a height $h = 0.25$ mm. Only the outer rim of the annulus is in contact with the CSTR contents. This design makes it possible to observe the color changes across the 1.00 mm width of the flat annulus (Figure 1). The volume of the CSTR is $V = 25$ cm^3. The residence time $\tau = 600$ s and the CSTR temperature $T = 25$ °C were kept constant. The feed is provided by three separate streams of chemicals, injected by precision pumps (Pharmacia P 500), that enter the CSTR by a single inlet port. Two streams respectively contain fixed concentrations of sodium chlorite (Prolabo, 96% purity) and potassium tetrathionate (Fluka) stabilized in 3×10^{-4} M NaOH solutions. Variable amounts of perchloric acid and sodium hydroxide are added through the third stream to control the pH of the input solutions. This is done by pumping different volume ratios of acid and base, keeping the overall flow rate constant. For experimental and graphic convenience, this relative distribution is characterized by a control parameter α on which the acid and the base flow concentrations depend linearly: respectively as $[HClO_4]_0 = \alpha \times [HClO_4]_{res}$, $[NaOH]_0 = (1 - \alpha) \times [NaOH]_{res}$, where $[HClO_4]_{res}$ and $[NaOH]_{res}$ are the acid and base feed concentrations from the reservoirs which were respectively fixed to 0.33×10^{-2} and 1.67×10^{-2} mol/dm^3. The pH of the feed mixture decreases as α increases from 0 to 1. To reduce the effective diffusivity of protons, controlled amounts of sodium poly(acrylate) (PA) (Polyscience, 20000D) are also added through this third stream. The solutions contain bromophenol blue, a pH color indicator that changes from purple-blue (basic) to

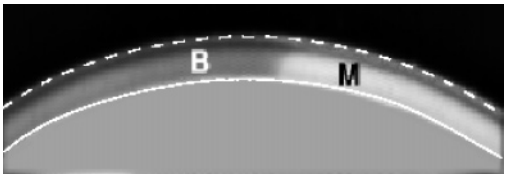

Figure 2. Illustration of an interface between the stable B state (left) and the stable M state (right) in an annular gel OSFR (between white dash lines). For experimental conditions, see text.

yellow-orange (acid) around pH = 3.8. In the following, the bracketed terms $[X]_0$ are the concentration that the species X would have in a collective feed-stream, prior to any reaction. The fixed values of $[NaClO_2]_0$ and $[K_2S_4O_6]_0$ are respectively 1.9×10^{-2} and 0.5×10^{-2} mol/dm^3. In experiments with PA, the gel reactors are set in contact with solutions of appropriate poly(acrylate) concentrations for a day before starting the experiment to let the macromolecule diffuse into the agarose matrix. The chemical state of the CSTR is monitored by the redox potential of a bright platinum electrode. The color profiles of stationary states and wave patterns in the gel are monitored by a CCD camera and the dynamics are recorded on a time-lapse VCR. A frame grabber digitizes the images for further processing.

Experimental Results

Under our experimental conditions, the CT reaction operated in a CSTR exhibits bistability between a branch B of basic states (pH $\sim$ 10), and a branch A of acid states (pH $\sim$ 2).[22,23] The CSTR contents are maintained on the branch of B-states. Different states can be observed in the gel depending on α and on the initial pH conditions of the gel, as shown in previous publications.[22,23] If the gel is initially acid, and if α is slightly lower than the value corresponding to the limit of stability of the CSTR B branch, the inner part of the gel remains acid while the part in contact with the CSTR contents becomes basic. A sharp front forms parallel to the gel/CSTR contact surface between the basic boundary layer and the acid core. This state of the gel is referred to as the mixed state or state M (Figure 2). On decreasing α, state M remains stable over some range of this parameter. However, the radial extension of the basic peripheral zone eventually starts to grow. At a critical value, the acid/base front becomes unstable and starts to oscillate. In this oscillatory regime, the front between the basic and the acid part moves back and forth in the radial direction. The parameter domain over which these surprising oscillations are observed is usually very small (a few percent of the parameter domain over which the stable M state is observed). On decreasing α beyond this oscillatory region, the gel turns completely basic. It was shown[22,23] that in this case the composition of the gel does not significantly differ from that of the CSTR and so, by extension, we call this the B state of the gel (Figure 2). A further decrease of α brings no qualitative change in the state of the gel. Now, on increasing α the B state of the gel remains stable until the branch of CSTR basic states loses stability. Thus, there is a region of parameter space over which states B and M coexist in the gel. This defines the domain of spatial bistability. In this domain, it is possible to prepare[29] different parts of the gel in either state. It is then possible to test their relative stability and to study the geometric properties of the M−B interface. Figure 2 is an illustration of such an interface between state B (the quasi-uniform dark-gray left portion of the gel) and state M (the right portion of the gel with a sharp switch from dark to pale gray). Note that, consistent with a no-flux boundary condition, the connection of the acid/base switch is orthogonal to the impermeable wall at the bottom of the groove. Thus, the acid region which makes the difference between state M and state B naturally develops a curvature at the interface.

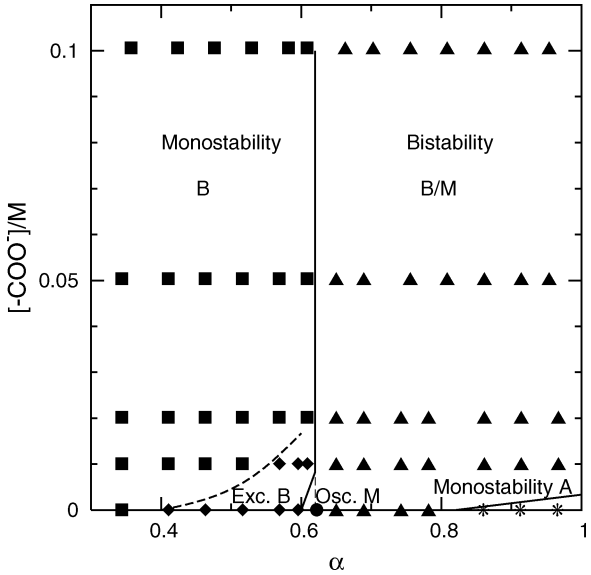

Figure 3. Experimental phase diagram in the ($[OH^-]_0$, $[-COO^-]_0$) plane ($-COO^-$ functions from poly(acrylate)), observed in the annular OSFR. The symbols correspond the experimental points and are attributed to states of the gel: (■) monostable (nonexcitable B state); (◆) monostable (excitable B state); (▲) bistable (stationary B/M state); (●) bistable (stationary B state/oscillatory M state); (∗) CSTR contents switches to the thermodynamic state.

In the range of α corresponding to the spatial-bistability domain, one would expect that one of the stationary states would expand at the expense of the other, the direction of expansion depending on the value of α. We have systematically probed this relative stability of states, as a function of α and for different concentrations of poly(carboxylic acid) in the feed solution. In the absence of carboxylated polymer chains, the M state always takes over the B state, even at the very limit of the domain of stability of the M state at low α. In fact, even when the B state is the only asymptotically stable state, an acid perturbation of this state can lead to a M−B-state-like interface that propagates undamped into the B state. However, behind this interface the acid region survives only a short period of time. Ultimately, the B state totally recovers. A traveling pulse forms. This property defines an excitable B state. Excitability of the B state extends some distance beyond the limit of the spatial bistability domain.

We have studied the stability domains of the B and M states in the (α, $[PA]_0$) plane and systematically tested the response of the B state to local acid perturbations. The results are gathered in a phase diagram (Figure 3). Excitability of the state B rapidly decreases as the polycarboxylate ion concentration increases in the feed. For concentrations of carboxylic functions above 0.02 mol/dm^3 no traveling acid pulse is observed in the monostability domain of state B. In the present experimental conditions and within our experimental accuracy, the oscillatory M state is not detected when 0.01 mol/dm^3 of carboxylate functions are introduced in the feed. Remarkably, the stability limit of the stationary state M, at low α, does not depend on the concentration of proton-complexing sites (i.e., carboxylate functions). This limit ranges between 0.6 and 0.62. However, the high-α stability limit shifts out of our experimental range with the rapid increase of stability of state B with increased poly(acrylate) in the feed.

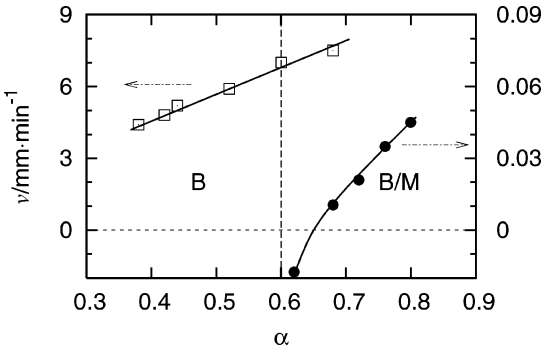

Figure 4. Propagation velocity of the M−B states interface, in the annular OSFR, as a function of α: (□) in the absence of carboxylic groups (left "*y*" scale); (●) in the presence of $[-COO^-]_0 = 0.1$ mol/dm^3 (from poly(acrylate))(right "*y*" scale).

Figure 4 illustrates the qualitative and quantitative changes induced by the introduction of PA on the relative stability of states. In the absence of poly(acrylate), the M state always propagates into the B state, when α is within the spatial bistability range. We count as positive this direction of interface propagation. The interface velocity decreases with decreasing α but never changes sign. In the domain where the B state is excitable, the velocity dependence of an acid pulse on α is in perfect continuation (no curve break) with the values obtained in the spatial bistability domain, except that the gel contents now ultimately returns to the B state. This indicates that, in first approximation, the front velocity is affected only by the concentrations ahead of the front and not by the recovery process, except maybe very close to the pulse propagation limit $\alpha \simeq 0.37$. Below this limit, any acid perturbation decays.

In the presence of poly(acrylate) the velocity of propagation dramatically slows down. At 0.1 mol/dm^3 of carboxylate groups the velocity is 100 times slower than in the absence of this proton-binding agent (Figure 4). More interestingly, within the spatial bistability range, the velocity of the interface changes sign as a function of α.

The velocity of the M−B interface drops to values close to zero at the limit of stability of the M state when the concentration of acrylate functions reaches approximatively 0.02 mol/dm^3. The introduction of a reversible binding agent for protons quenches the excitability properties of the B state. The standard qualitative behavior of spatial bistable systems is recovered with the addition of a high enough quantity of PA: in the bistability domain the direction of the propagation of an interface between the two steady states changes for a critical parameter value. This result supports the assumption that the oscillatory and excitability properties of the CT reaction operated in an OSFR are linked to long-range activation by migrating protons and are not the direct result of the reaction kinetic mechanism.

Previous experimental observations[25] and theoretical calculations[24] have shown that, in standard spatial bistable conditions, the critical control parameter value at which the relative stability of spatial steady states changes can sensitively depend on the width of the OSFR. In connection with the quest for chemomechanical instabilities,[30] the study of the relative stability of states as a function of the width *w* of the OSFR is of fundamental interest. However, in our annular OSFR with a height $h = 0.25$ mm, negative propagation velocities of the M−B state interface are difficult to detect. The critical switching value as a function of α remains very close to that of the limit of stability of state M, and the interface velocities remain very small. Furthermore, because bromophenol blue is slowly bleached by chlorine-dioxide produced in the acid/base front,[31] these slow interfaces are very fuzzy and difficult to follow, especially when the optical path across the piece of gel is only a few tenths of millimeters.

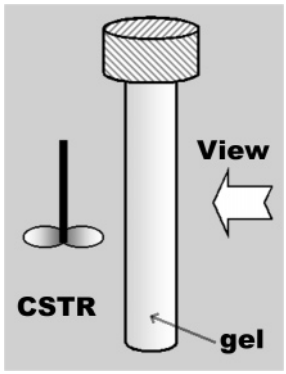

Figure 5. Sketch of the gel core of a cylindrical OSFR.

To solve the above interface-detection problem and to test the sensitivity of the relative stability of states B and M on the width of an OSFR, additional experiments were performed in a cylindrical-gel OSFR (Figure 5). Cylindrical, conical,[32,33] and spherical[34] pieces of gel uniformly fed at their surface can also be considered as one-side-fed-reactors with the difference that the curvature of the feed surface must be taken into account. Long thin cylindrical-gel OSFRs are easier to produce and handle than flat annular gels. In addition, in the cylindrical geometry, the absorbance of the dye is integrated over the diameter of the cylinder which typically ranges from 1.0 to 2.0 mm, to compare to the 0.25 mm in the flat annular OSFR. Thus, in the axial direction, the color contrast between the two spatial states is much improved. However, the advantages of the periodic boundary conditions of annular gels are lost.

For the cylindrical-gel OSFR experiments, the 2% agarose gel is initially cast in silicon tubes of different diameters. After being removed from their mold, each cylinder is then soaked for at least 24 h in a 0.7% sodium poly(acrylate) aqueous solution (corresponding to a concentration of 7.65×10^{-2} mol/dm^3 carboxylate groups) before being glued onto a stopper and introduced at the top of a tall cylindrical CSTR designed for fast recirculation of the contents from bottom to top (Figure 5). The gel cylinders are totally immersed in the solution. The new CSTR, made of polished transparent Plexiglas, has a volume of 46 cm^3, a residence time of 600 s, and is thermoregulated at 25 or 35 °C—as appropriately indicated in the captions. The feed concentrations of the reagents are the same as above and a fixed concentration of PA corresponding to 7.65×10^{-2} mol/dm^3 of carboxylate groups is injected in the CSTR. However, to fit with the experimental conditions of parallel studies on size-responsive gels, no acid + base mixtures are injected through the third feed channel. Only variable additional amounts of NaOH are injected through this channel and are used as the control parameter. Note that, an increase in $[NaOH]_0$ corresponds to a decrease in α. Also, for practical reasons, the pH indicator is changed to methyl-red (Aldrich), which turns from clear yellow to dark-red when the solution switches from basic to acid. Thus, the dark acid states in the cylinder of gel are more easily observable across the clear alkaline contents of the CSTR. The state of the CSTR is accurately monitored by a pH electrode.

The snapshots in Figure 6 show the propagation of the M state, characterized by an acid core (dark gray), into the alkaline (clearer) B state, respectively in the positive (a−c) and the negative (d−f) directions inside a OSFR with a radius $r = 0.5$ mm. Note that for positive values (M state propagating into the

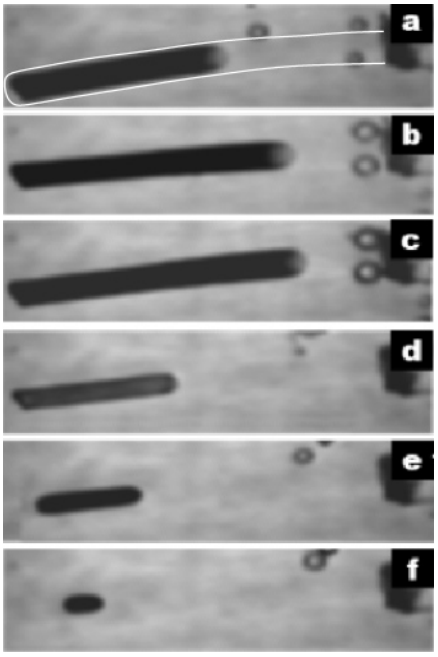

Figure 6. Sequences of snapshots illustrating the propagation of M−B interfaces in the cylindrical OSFR (top of the cylinder on the left and bottom on the right): (a−c) $[OH^-]_0 = 1.3 \times 10^{-3}$ mol/dm^3, interface velocity +5.1 mm/h; (d−f) $[OH^-]_0 = 2.3 \times 10^{-3}$ mol/dm^3, interface velocity −2.4 mm/h. Conditions: diameter of the gel cylinder 1 mm, temperature 25 °C, and $[-COO^-]_0 = 7.65 \times 10^{-2}$ mol/dm^3 (from poly(acrylate)); for other parameters, see text. The gel boundary, not visible in the snapshot, is schematically drawn in snapshot a.

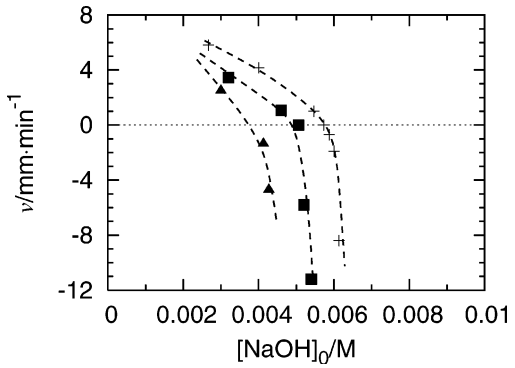

Figure 7. Propagation velocities of the M−B interface as a function of $[NaOH]_0$ in cylindrical OSFRs of different diameters: (△) 1 mm; (□) 1.5 mm; (+) 2 mm. Conditions: $[-COO^-]_0 = 7.65 \times 10^{-2}$ mol/dm^3 (from poly(acrylate)) and a temperature of 35 °C; for other parameter values, see text.

B state) the acid core is significantly broader than for the negative values (B state propagating into the M state). These changes of state characteristics in the radial direction are in agreement with previous observations in other systems.[24,25] In this range of radius (or width), the high $[NaOH]_0$ (low α) limits of the spatial bistability strongly depend on the radial size of the OSFR,[23] and as illustrated (Figure 7), the value of $[NaOH]_0$ at which the M−B interface velocity changes direction decreases with the decrease of the radius of the cylinder of gel.

Numerical Results and Discussion

Numerical simulations based on the kinetic model presented earlier were performed in complement to experiments. It was previously shown[22,23] that, in the absence of complexing agent, the dynamical properties of the CT reaction in a OSFR can be accounted for almost quantitatively by eqs 1, 3, and 4 with the

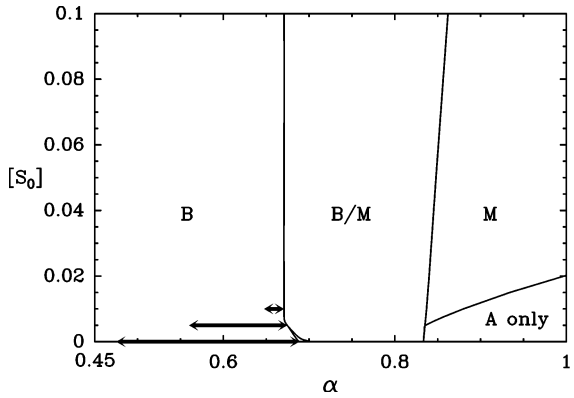

Figure 8. Computed stability diagram in the plane (α,[S_0]). A zoom on the oscillatory domain is given in Figure 9.

associated rate laws (eqs 2, 5, and 6). The following values were used for the kinetic constants: $k = 5 \times 10^6$ M^{-3} s^{-1}, $k_e^- = 1.4 \times 10^{11}$ M s^{-1}, and $k_e^+ = K_e\, k_e^-$ with $K_e = 10^{-14}$, $k_a^- = 10^{11}$ M s^{-1}, and $k_a^+ = K_a\, k_a^-$ with $pK_a = -\log(K_a) = 1.94$. The chemical feeds and other essential parameters were taken to fit the experimental conditions of the annular OSFR. The residence time of the CSTR is $\tau = 600$ s. The ratio of the volume of the gel to the volume of the CSTR is 1.75×10^{-3} for a 1 mm width. The concentrations in the input flow are $[ClO_2^-]_0 = 2 \times 10^{-2}$ M and $[S_4O_6^{2-}]_0 = 5 \times 10^{-3}$ M, and α is defined as in the experiments. To account for the fast diffusion of H^+ and OH^-, their diffusion coefficients were fixed to $D_{fast} = 3.4 \times 10^{-5}$ cm^2 s^{-1} and all the other coefficients to a standard value $D = 10^{-5}$ cm^2 s^{-1}. The value of D_{fast} is an effective coefficient that was set by a previous[22,23] fit of a few experimental data. This effective value accounts both for the high diffusion coefficient of these ions and for the electrostatic effect of the other ions on the fast charged species. To include the effects of a complexing agent, we introduce an additional fast equilibrium with a species S^-:

$$H^+ + S^- \rightleftharpoons HS \tag{7}$$

with rate law:

$$v_s = k_s^+[HS] - k_s^-[H^+][S^-] \tag{8}$$

with $k_s^- = 10^{11}$ M s^{-1} and $k_s^+ = K_s\, k_s^-$ and $pK_s = -\log(K_s) = 5.5$.

Diagrams of stability and boundaries of oscillatory domains were computed in 1-D simulations, while the excitability domains were determined in 2-D simulations. More details on the numerical procedures are found in refs 23 and 33.

The computed phase diagram in the plane (α, S_0), where S_0 is the total amount of available immobile complexing sites for protons, is given in Figure 8. Figure 9, is a zoom of the small domain of oscillatory M state. The double arrows in Figure 8 delimit the domain of excitable B state for a few values of S_0. At $S_0 = 2 \times 10^{-2}$ M, this state is no longer found to be excitable. Despite the simplicity of the model, the results are in good, almost quantitative, agreement with the experimental results. Except for small values of S_0 where the B → M transition cannot be distinguished from the B → A transition of the CSTR contents, the former transition occurs before the latter. When S_0 increases, this B → A transition is shifted to higher values of α, but, since the experimental procedure restricts the range to $\alpha \leq 1$, this limit is out of reach beyond $S_0 \sim 2 \times 10^{-2}$ M. Let us now focus on the stability limit of the M state at low α.

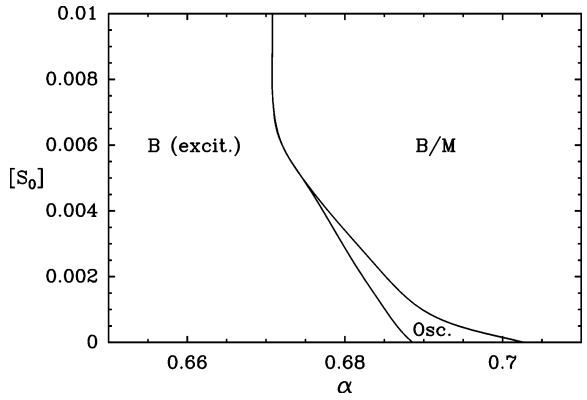

Figure 9. Detail of the stability diagram given in Figure 8: limits of the oscillatory domain.

At $S_0 = 0$, on decreasing α, the M state develops a small domain of oscillations just before disappearing (Figure 9). In the model, these oscillations were shown to result from the long-range activation linked by the fast diffusion of H^+ and have been extensively discussed in ref 23. For the same reasons, outside the bistability domain, the B state remains excitable over a large domain of parameters ($0.475 < \alpha < 0.69$). When the complexing agent is introduced, the effective diffusion of H^+ is divided by a factor $\sigma = 1 + S_0/K_s$.[8] As a consequence, the extent of the domains of oscillations and of excitability decrease when S_0 increases. These behaviors have totally vanished at $S_0 = 2 \times 10^{-2}$ M. Numerical results are quantitatively consistent with experimental determinations. In both cases, for $S_0 \geq 2 \times 10^{-2}$ M, the stability limit of the M state exhibits a remarkable invariance as a function of S_0. This surprising behavior can be understood in the following way. On the basis of simple arguments, it was previously shown[24] that if the front of the M state is sharp and a substrate (here OH^-) is almost completely transformed, the distance δ of this front to the CSTR boundary is approximately given by the following relation:

$$\delta \propto \frac{DX}{\dot{Q}} \tag{9}$$

X is the concentration of the substrate at the feed-boundary, D the diffusion coefficient of the driving species (here H^+), and $\dot{Q}$ is the rate of consumption of the substrate. This distance does not depend on the width w of the system. State M loses its stability when w becomes of the same order as δ. When a certain amount of complexing agent is added, the effective diffusion D and the reaction rate $\dot{Q}$ of the autocatalytic reaction are both divided by the same factor σ. Thus, according to eq 9, δ remains unchanged. It was checked during the computations that for a given α the distance δ is independent of S_0 and w provided that S_0 is large enough to avoid long-range activation effects. Because δ only depends on α (through X) and for a given w M loses stability when δ reaches a critical value (of order w), the transition point does not depend on S_0. This invariance is similar to the result obtained by Pearson and Bruno[9] for the threshold of Turing structures. On the same basis, they show that this threshold is independent of the concentration of the complexing agent used to slow the diffusion of the activator. Obviously, this does not infer that S_0 has no effect on the dynamics. Although the position of the transition is unchanged, the system dynamics can be dramatically slowed and the concentration profiles of the two different stable states are modified.

Within the bistable domain and for low concentrations of the binding agent, state M invades state B when these two states are in contact; i.e., the M state is more stable than the B state. However, it was shown in the experiments that, for high enough values of S_0, the propagation velocity can be reversed in the vicinity of the bistability limit. To check this point without undertaking too lengthly calculations, we have used a smaller width $w = 0.3$ mm to decrease the relaxation times, and a value $S_0 = 10^{-1}$ M. With these parameters the bistability limit is located at $\alpha \simeq 0.715$. The shift to higher α (lower $[OH^-]_0$) with decreasing width follows the experimental observations (Figure 7). In the bistability domain, at $\alpha = 0.73$, state M still invades state B with a propagation velocity equal to 1.27×10^{-4} mm/s. However closer to the bistability limit the situation is reversed, for $\alpha = 0.72$, state B invades state M at a velocity equal to 6.1×10^{-5} mm/s.

Conclusion

This report confirms that the oscillatory and the excitability properties of the CT reaction operated in an OSFR are induced by long-range-activation instabilities. The interface dynamic of standard bistable systems is recovered when the diffusivity of the protons—the activatory species—is selectively and sufficiently slowed. The addition of large enough amounts of poly(acrylate) ions can even make the system short range activated. This is clearly shown to occur for concentrations of quasi immobile carboxylic functions above 2×10^{-2} M. Note that the different steps taken above: the characterization of a spatial bistability domain, the search for conditions where the direction of propagation of interfaces between the two spatial steady states changes sign, and the development of effective short-range activation are the first steps in a recently proposed systematic method to produce stationary pulse patterns of one state immersed into an other state (domain patterns). The final step of the method is to study head-on collisions of spatial interfaces in a range of parameters near to the values where the direction of propagation of the spatial interface changes sign and search for conditions where nonvanishing front pairing would form. With this possibility in mind, we studied the collision dynamics of spatial interfaces having slow positive velocities for a concentration of acrylate function equal to 0.1 mol/dm^3; the goal was to observe stationary pulses of the B state localized in the M state. Up to now, this quest is not successful. Beside the fact that we have explored only a small range of possible feed parameters, the bleaching of the color dye in the acid/base front, makes the observation of a narrow region of the B state difficult. Furthermore, a recent kinetic investigation[31] shows that chloride ions can play a secondary activatory role in the CT reaction. The diffusivity of this species is not affected by the introduction of poly(acrylate) and the slow head-on collisions of the spatial state interfaces could not be prevented in these conditions. We now continue the quest for stationary patterns in other pH-activated systems, like the iodate−sulfite reaction, where we expect to avoid the above difficulties.

Acknowledgment. This research has been supported by a Marie Curie Fellowship of the European Community program Improving Human Potential under contract number HPMF−CT-2002-011771. We thanks the support of the ESF "REACTOR" program. I.S. expresses thanks for the support of the Hungarian Academy of Sciences (HAS) (F049666, T0437473).

References and Notes

(1) Field, R. J., Burger, M., Eds. *Oscillations and Traveling Waves in Chemical Systems*; Wiley: New York, 1985.

(2) Kapral, R., Showalter, K., Eds. *Chemical Patterns and Waves*; Kluwer Academic Publisher: Amsterdam, 1995.

(3) Epstein, I. R.; Pojman, J. *An Introduction to Nonlinear Chemical Dynamics*; Oxford University Press: New York, 1988.

(4) Murray, J. D. *Mathematical Biology I.-II.*; Springer-Verlag: Berlin, 2002.

(5) Borckmans, P.; Dewel, G.; De Wit, A.; Dulos, E.; Boissonade, J.; Gauffre, F.; De Kepper, P. *Int. J. Bif. Chaos* **2002**, *12*, 2307.

(6) Sagues, F.; Epstein, I. R. *Dalton Trans.* **2003**, 1201.

(7) Turing, A. M. *Philos. Trans. R. Soc. London, Ser. B* **1952**, *23*, 737.

(8) Lengyel, I.; Epstein, I. R. *Proc. Natl. Acad. Sci. U.S.A.* **1992**, *89*, 3977.

(9) Pearson, J. E.; Bruno, W. J. *Chaos* **1992**, *2*, 513.

(10) Vanag, V. K.; Epstein, I. R. *Science* **2001**, *294*, 835.

(11) Lengyel, I.; Rábai, G.; Esptein, I. R. *J. Am. Chem. Soc.* **1990**, *112*, 4606.

(12) Castets, V.; Dulos, E.; Boissonade, J.; De Kepper, P. *Phys. Rev. Lett.***1990**, *64*, 2953.

(13) Ouyang, Q.; Swinney, H. L. *Nature* **1991**, *352*, 610−612.

(14) Davies, P. W.; Blanchedeau, P.; Dulos, E.; De Kepper, P. *J. Phys. Chem.* **1998**, *102*, 8236. Rudovics, B.; Barillot, E.; Davies, P. W.; Dulos, E.; Boissonade, J.; De Kepper, P. *J. Phys. Chem.* **1999**, *103*, 1790.

(15) Szalai, I.; De Kepper, P. *J. Phys. Chem. A* **2004**, *108*, 5315.

(16) Lee, K. J.; McCormick, W. D.; Ouyang, Q.; Swinney, H. L. *Science* **1993**, *261*, 192.

(17) Edblom, E. C.; Orbán, M.; Epstein, I. R. *J. Am. Chem. Soc.* **1986**, *108*, 2826. Edblom, E. C.; Györgyi, L.; Orbán, M.; Epstein, I. R. *J. Am. Chem. Soc.* **1987**, *109*, 4876. Gáspár, V.; Showalter, K. *J. Am. Chem. Soc.* **1987**, *109*, 4869. Gáspár, V.; Showalter, K. *J. Phys. Chem.* **1990**, *94*, 4973.

(18) Tam, W. Y.; Horsthemke, W.; Noszticzius, Z.; Swinney, H. L. *J. Chem. Phys.* **1988**, *88*, 3395.

(19) Dulos, E.; Boissonade, J.; De Keppper, P. *Physica A* **1992**, *188*, 120.

(20) Ouyang, Q.; Flesselles, J. M. *Nature (London)* **1996**, *379*, 143.

(21) Petrov, V.; Quyang, Q.; Swinney, H. L. *Nature (London)* **1997**, *338*, 655. Lin, A. L.; Bertram, M.; Martinez, X.; Swinney, H. L. *Phys. Rev. Lett.* **2000**, *84*, 4240.

(22) Boissonade, J.; Dulos, E.; Gauffre, F.; Kuperman, M. N.; De Kepper, P. *Faraday Discuss.* **2001**, *120*, 353.

(23) Fuentes, M.; Kuperman, M. N.; Boissonade, J.; Dulos, E.; Gauffre, F.; De Kepper, P. *Phys. Rev. E* **2002**, *66*, 056205.

(24) Blanchedeau, P.; Boissonade, J. *Phys. Rev. Lett.* **1998**, *81*, 5007.

(25) Blanchedeau, P.; Boissonade, J.; De Kepper, P. *Physica D*, **2000**, *147*, 283.

(26) Nagypál, I.; Epstein, I. R. *J. Phys. Chem.* **1986**, *90*, 6285.

(27) Horváth, D.; Tóth, Á. *J. Chem. Phys.* **1998**, *108*, 1447.

(28) Jakab, É.; Horváth, D.; Tóth, Á.; Merkin, J. H.; Scott, S. K. *Chem. Phys. Lett.* **2001**, *342*, 317.

(29) This is done by briefly taking out of the CSTR the gels on their holders and making a local acid perturbation to a gel system initially uniformly in the B state.

(30) Gauffre, F.; Labrot, V.; Boissonade, J.; De Kepper, P. *ACS Symp. Ser.* **2004**, *869*, 80.

(31) Horvath, A. K.; Nagypal, I.; Peintler, G.; Epstein, I. R. *J. Am. Chem. Soc.* **2004**, *126*, 6246.

(32) Gauffre, F.; Labrot, V.; Boissonade, J.; De Kepper, P.; Dulos, E. *J. Phys. Chem.* **2003**, *107*, 4452.

(33) Strier, D.; Boissonade, J. *Phys. Rev. E* **2004**, *70*, 016210.

(34) Boissonade, J. *Phys. Rev. Lett.* **2003**, *70*, 188302.